

Article

The Chaotic-Based Control of Three-Port Isolated Bidirectional DC/DC Converters for Electric and Hybrid Vehicles

Zheng Wang ^{1,*}, Bochen Liu ¹, Yue Zhang ¹, Ming Cheng ¹, Kai Chu ¹ and Liang Xu ²

¹ School of Electrical Engineering, Southeast University, Nanjing 210096, China; bcliu@seu.edu.cn (B.L.); yuezhang@nuaa.edu.cn (Y.Z.); mcheng@seu.edu.cn (M.C.); chukai1991@163.com (K.C.)

² Aviation Key Laboratory of Science and Technology on Aerospace Electromechanical System Integration, No. 33 Shuige Road, Jiangning District, Nanjing 210061, China; xlp1983@163.com

* Correspondence: zwang@eee.hku.hk or zwang@seu.edu.cn; Tel.: +86-137-7079-6825

Academic Editor: Joeri Van Mierlo

Received: 31 July 2015; Accepted: 13 January 2016; Published: 27 January 2016

Abstract: Three-port isolated (TPI) bidirectional DC/DC converters have three energy ports and offer advantages of large voltage gain, galvanic isolation ability and high power density. For this reason this kind of converters are suitable to connect different energy sources and loads in electric and hybrid vehicles. The purpose of this paper is to propose chaotic modulation and the related control scheme for TPI bidirectional DC/DC converters, in such a way that the switching harmonic peaks can be suppressed in spectrum and the conducted electromagnetic interference (EMI) is reduced. Two chaotic modulation strategies, namely the continuously chaotic modulation and the discretely chaotic modulation are presented. These two chaotic modulation strategies are applied for TPI bidirectional DC/DC converters with shifted-phase angle based control and phase-shifted PWM control. Both simulation and experiments are given to verify the validity of the proposed chaotic modulation-based control schemes.

Keywords: electric and hybrid vehicles; energy conversion; bidirectional DC/DC converter; chaotic modulation; shifted-phase angle based control

1. Introduction

With the increasing problems of emissions from oil/gas powered vehicles and the decreasing availability of fossil fuels around the world, electric vehicles (EVs) and hybrid electric vehicles (HEVs) are gaining widespread attention nowadays [1,2]. EVs and HEVs not only save fossil fuel, but also achieve low gas emissions for environmental protection [3]. Emerging renewable energy techniques have been introduced in EVs [4]. In EVs and HEVs, the bidirectional DC/DC converter is a prominent option to exchange power between the low-voltage energy storage device and the high-voltage DC bus of the traction motor [5]. In Figure 1a, a bidirectional DC/DC converter is used to exchange power between the battery and the high-voltage DC bus in series of a HEV, in such a way that the DC link voltage is kept stable despite of voltage changes in the battery and load variation in the traction motor [6]. Figure 1b plots the configuration of a dual-active-bridge (DAB) isolated DC/DC converter, which is used to connect the battery and the DC bus of the traction motor [5]. Besides, the bidirectional DC/DC converter can be used to exchange power between the battery and the grid to satisfy the requirements of vehicle-to-grid (V2G) operation of EVs, which is shown in Figure 2 [7,8].

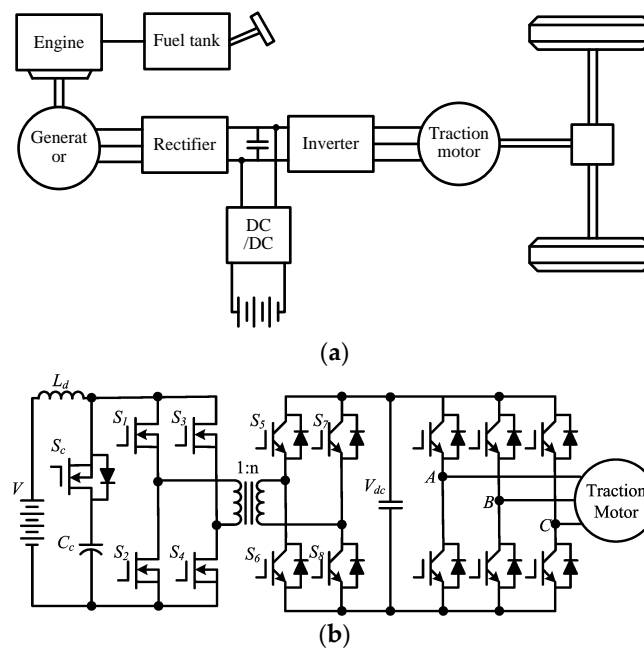


Figure 1. Energy conversion system in series HEV with bidirectional DC/DC converter: (a) system configuration; (b) DAB converter.

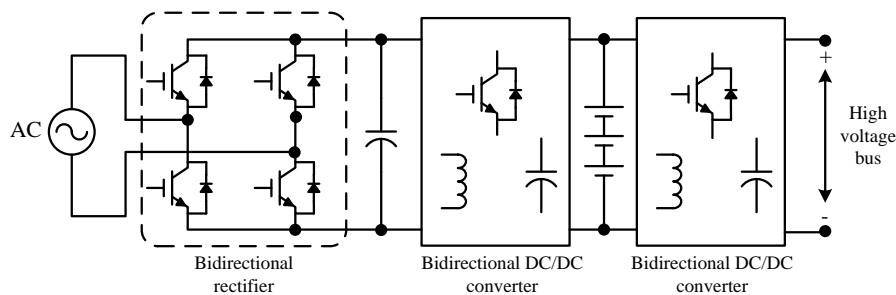


Figure 2. Electric charging system for V2G of EV.

Bidirectional DC/DC converters can be classified into isolated converters and non-isolated converters [9,10]. Non-isolated converters usually have simple topologies and fewer components, but they face challenges in high-gain voltage conversion and galvanic isolation. On the other hand, isolated converters can achieve wide-range voltage conversion and electric isolation by using high-frequency transformers [5,11–14]. Different from two-port bidirectional DC/DC converters, multi-port DC/DC converters are derived to exchange power among multiple DC ports. In [15], a multi-input non-isolated DC/DC converter is proposed for hybrid energy sources in fuel cell electric vehicles, where three energy sources are connected to a common DC bus through separate buck/boost converters. Figure 3 shows the system configuration in [15]. In [16], a partially isolated multi-port DC/DC converter is proposed to achieve power conversion among different DC ports in hybrid vehicles. For this configuration, a non-isolated bidirectional half-bridge DC/DC converter is used to exchange power between two energy sources, and an isolated dual half-bridge DC/DC converter is used to exchange power between the energy sources and the traction motor. Only four active switching devices are needed since the two energy sources share one half-bridge leg on primary side of the high-frequency transformer. Similarly, another partially isolated multi-port DC/DC converter is proposed by using separate bidirectional half-bridge DC/DC converters for two energy sources, and high controllability is provided for power conditioning [17].

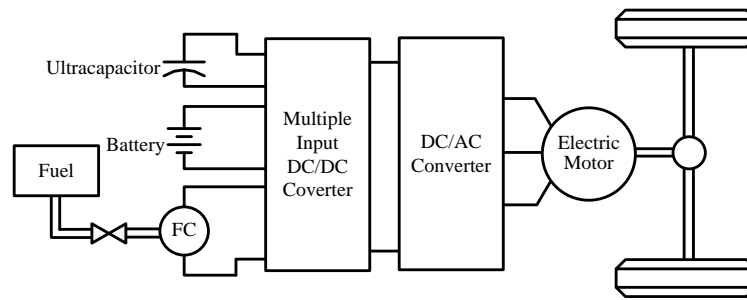


Figure 3. System configuration of fuel cell electric vehicles using multi-input DC/DC converter.

Different from the aforementioned multi-port converters based on two-winding transformers, a three-port isolated (TPI) bidirectional DC/DC converter is proposed for three energy ports by integrating three windings magnetically [18–20]. As an isolated DC/DC converter, the TPI bidirectional DC/DC converter has the features of high-gain voltage conversion and electric isolation [5]. The zero voltage transition (ZVS) condition can be achieved by the leakage inductances of transformer and parasitic capacitance of switching devices. Due to the reduction of switching losses with ZVS operation, the switching frequency of TPI bidirectional DC/DC converter is increased. Previously, several examples of TPI bidirectional DC/DC converters have been given. In [18], the shifted-phase angle based control is deduced to control power for the TPI bidirectional DC/DC converter. In [19], the shifted-phase angle based control is further applied for a triple-half-bridge based TPI bidirectional DC/DC converter, which is used for the hybrid energy source consisting of fuel cells and super-capacitors. In [20], a decoupled power flow control scheme is proposed to mitigate the coupling effects among different ports of the TPI bidirectional DC/DC converter by linearizing the power at the operating points. In [21], the TPI bidirectional DC/DC converter is used to connect different batteries to a grid inverter for battery charging in EV. To the best of authors' knowledge, all the previous work on TPI bidirectional DC/DC converters are with fixed switching-frequency, where the peak harmonics are clustered around the switching-frequency and its multiple values in spectrum. These peak switching harmonics may induce conducted electromagnetic interference (EMI) in power converters [22].

Different from the fixed switching-frequency based control, the aim of this paper is to propose chaotic modulation strategies and the related control schemes for TPI bidirectional DC/DC converters, in such a way that the switching harmonic peaks can be suppressed in spectrum and the conducted EMI is reduced in EVs. By changing the switching frequency chaotically, the distinct switching harmonic peaks with fixed switching-frequency are broken and the power can be spread out within the nearby domain in spectrum. Either the random or chaotic modulation has been studied in various power converters [22–24], but those works are mainly focused on one single converter. Due to the existence of three power converters in a TPI bidirectional DC/DC converter, the chaotic modulation strategy should be designed collaboratively for the three energy ports for stable operation. Two chaotic modulation strategies, namely the continuously chaotic modulation and the discretely chaotic modulation are proposed in this paper. They are applied to the shifted-phase angle based control and the phase-shifted PWM control for the TPI bidirectional DC/DC converter. Both simulation and experiments are given to verify the validity of the proposed schemes.

2. Operation Principle

Figure 4 shows the topology of a TPI bidirectional DC/DC converter. The three energy sources are connected to a three-port high-frequency transformer with full-bridge DC/DC converters. As shown in Figure 4, u_1 , u_2 and u_3 are converter output voltages of three ports, and i_1 , i_2 and i_3 are input currents of three ports. Figure 5a shows the equivalent model for the TPI bidirectional DC/DC converter. L_1 , L_2 and L_3 are leakage inductances of three ports, and L_m is the magnetic inductance. Figure 5b shows

the simplified Y-type equivalent model without magnetic inductance. L'_2 and L'_3 are the equivalent inductance values of L_2 and L_3 , which are observed from port 1. After converting the model from Y-type to Δ -type, Figure 5c is obtained. In Figure 5c, L_{12} is the equivalent inductance between port 1 and port 2, L_{13} is the equivalent inductance between port 1 and port 3, and L_{23} is the equivalent inductance between port 2 and port 3. The values of L_{12} , L_{13} and L_{23} are deduced as shown in Equation (1):

$$\left\{ \begin{array}{l} L'_2 = \frac{L_2}{n_2^2} \\ L'_3 = \frac{L_3}{n_3^2} \\ L_{12} = L_1 + L'_2 + \frac{L_1 L'_2}{L'_3} \\ L_{13} = L_1 + L'_3 + \frac{L_1 L'_3}{L'_2} \\ L_{23} = L'_2 + L'_3 + \frac{L'_2 L'_3}{L_1} \end{array} \right. \quad (1)$$

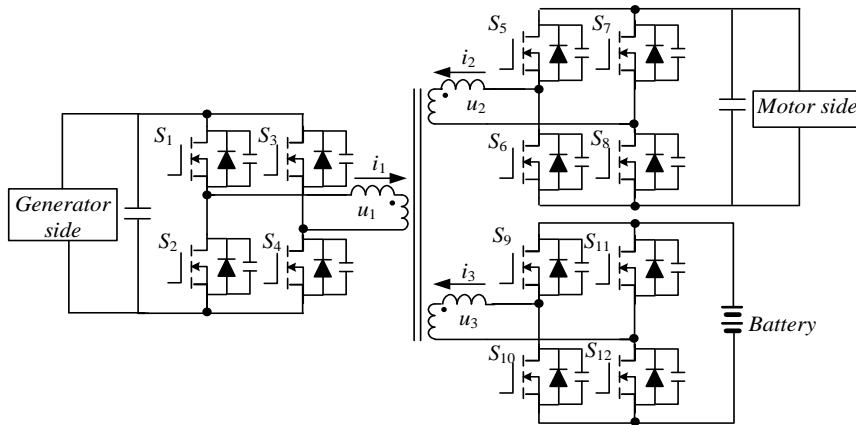


Figure 4. Configuration of TPI bidirectional DC-DC converter.

Based on the equivalent model in Figure 5c, the mathematical models of active power exchanged among three energy ports can be expressed in the following equations:

$$\left\{ \begin{array}{l} P_{12} = \frac{V_1 V'_2}{\omega L_{12}} \phi_{12} \left(1 - \frac{\phi_{12}}{\pi} \right) \\ P_{13} = \frac{V_1 V'_3}{\omega L_{13}} \phi_{13} \left(1 - \frac{\phi_{13}}{\pi} \right) \\ P_{12} = \frac{V'_2 V'_3}{\omega L_{23}} \phi_{32} \left(1 - \frac{\phi_{32}}{\pi} \right) \end{array} \right. \quad (2)$$

$$\left\{ \begin{array}{l} P_1 = P_{12} + P_{13} \\ P_2 = P_{12} + P_{32} \\ P_3 = P_{13} - P_{32} \end{array} \right. \quad (3)$$

where $\omega = 2\pi f$ and f is the switching frequency. ϕ_{12} is the shifted-phase angle between port 1 and port 2, ϕ_{13} is the shifted-phase angle between port 1 and port 3, and ϕ_{32} is the shifted-phase angle between port 2 and port 3, respectively. P_1 , P_2 and P_3 are active power of port 1, port 2 and port 3, respectively. From Equations (2) and (3), it can be observed that the exchanged power can be controlled by the shifted-phase angles between different energy ports.

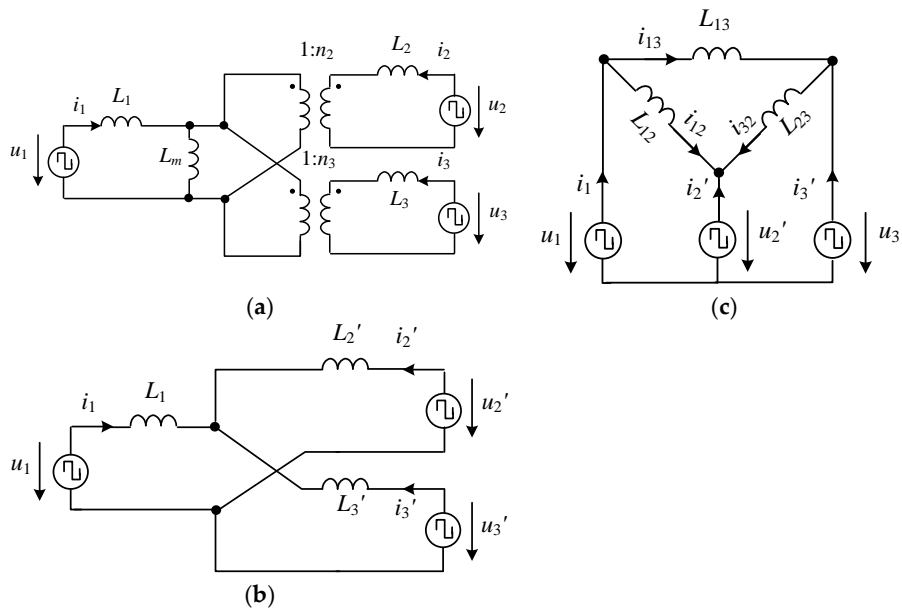


Figure 5. Equivalent model of TPI bidirectional DC/DC converter: (a) original equivalent model with magnetic inductance; (b) simplified Y-type equivalent model observed from port 1 without magnetic inductance; (c) simplified Δ -type equivalent mode.

Figure 6 plots the simulated steady-state waveforms of TPI bidirectional DC/DC converter with shifted-phase angle based control. A switching cycle is divided into 18 modes. The detailed working principle of the TPI bidirectional DC/DC converter is similar to the DAB isolated DC/DC converter. The ZVS operation is achieved when the anti-diode is freewheeling before the active switch takes the current [19]. By assuming $L_{12} = L_{13} = L_{32}$ and defining $d_{12} = u'_2/V_1$ and $d_{13} = u'_3/V_1$, the soft-switching operation conditions can be determined by the voltage gains d_{12} and d_{13} and shifted-phase angles ϕ_{12} and ϕ_{13} . As shown in Figure 7, the grey areas are the region for soft-switching conditions. To extend the soft-switching operation region, the PWM control can be incorporated in the shifted-phase angle control, and the phase-shifted PWM control is obtained [25]. This phase-shifted PWM control scheme can decrease the circulating current and increase the efficiency of the DC/DC converter [26].

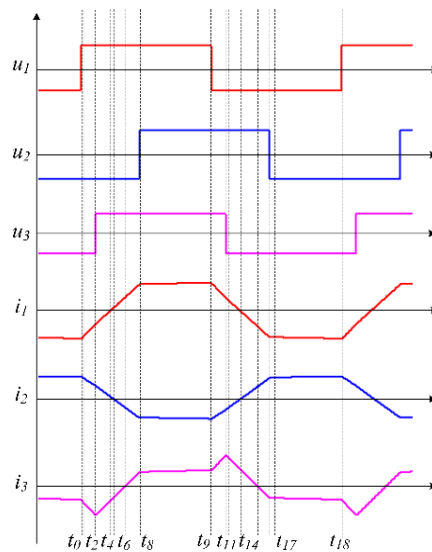


Figure 6. Simulated steady-state waveforms of TPI bidirectional DC/DC converter.

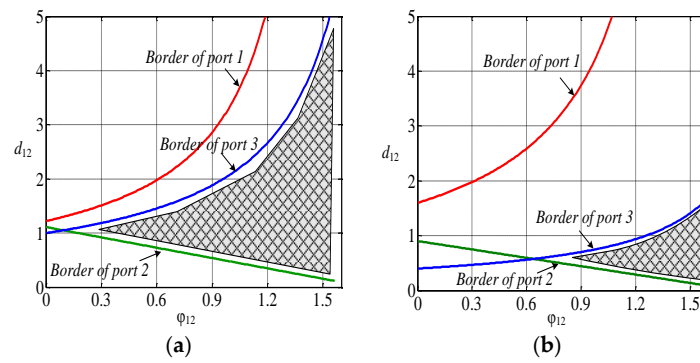


Figure 7. Soft-switching regions for TPI bidirectional DC/DC converter. (a) $\phi_{13} = \pi/9, d_{13} = 1$; (b) $\phi_{13} = \pi/6, d_{13} = 0.6$.

3. Chaotic Modulation

Chaotic modulation strategies have already been utilized to reduce the conducted EMI for power electronic converters and electric drives [22–24]. Due to the random-like features, chaotic modulation generates irregularly variable switching frequencies, which could be used to destroy the distinct switching harmonics and produce a continuous power spectrum. Chaotic modulation is easy to implement compared to a truly random source in practice. However, the previous studies on chaotic modulation were focused on a single power converter. Different from that, there are three full-bridge converters in the TPI bidirectional DC/DC converter. Therefore, a collaborative chaotic modulation design should be given for the three energy ports.

3.1. Generation of Chaotic Series

To chaotic the switching frequency of TPI bidirectional DC/DC converter, the chaotic series should be generated at first. The use of a logistic map is a simple and efficient approach to generate the chaotic sequence $\{x_i\}$:

$$x_{n+1} = F(A, x_n) = Ax_n(1 - x_n) \quad n = 1, 2, 3, \dots \quad (4)$$

where the control parameter $A \in [0, 4]$. Figure 8a depicts the bifurcation diagram of x_i versus A of the logistic map. The corresponding Lyapunov exponent versus A is shown in Figure 8b. It can be seen that when $A \in [0, 1)$, $\{x_i\}$ exhibits the zero value. When $A \in [1, 3)$, $\{x_i\}$ becomes a fixed value with $x_i > 0$. When A is further increased, $\{x_i\}$ begins to bifurcate with multiple values. When $A > 3.57$, $\{x_i\}$ exhibits infinite values. Besides, the boundary of these infinite values changes with the value of A . As the corresponding Lyapunov exponents are positive, it confirms that it is a chaotic series. Thus, by designing the value of A to be close to 4, the chaotic series $\{x_i\}$ will be distributed evenly within $(0, 1)$.

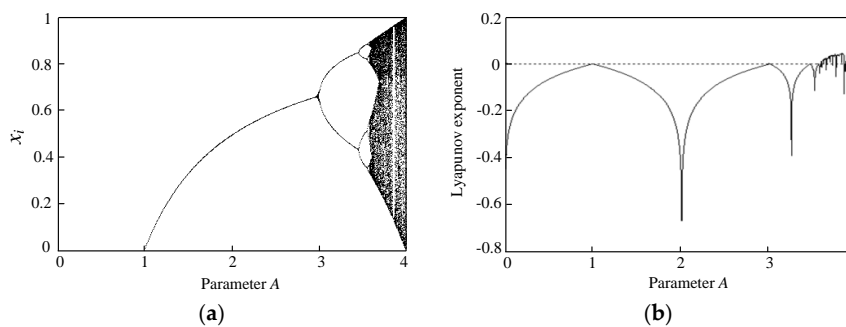


Figure 8. Logistic map: (a) bifurcation diagram; (b) Lyapunov exponents.

3.2. Chaotic-Frequency Switching Pulses

Based on the chaotic series $\{x_i\}$, two approaches, namely the continuously chaotic modulation and the discretely chaotic modulation are proposed to generate the chaotic pulses. As aforementioned, the shifted-phase angle can be used to regulate the power exchange for TPI bidirectional DC/DC converters. The duty ratio is kept as a constant value of 0.5 to ensure the symmetric operation of full-bridge of each port. Figure 9 shows principle of the continuously chaotic modulation strategy, where a sawtooth carrier wave is compared with a constant value of 0.5. The frequency of the sawtooth carrier wave is choaized by using the chaotic series $\{x_i\}$ as:

$$f = f_s + (2x_n - 1) \Delta f \tag{5}$$

where x_n is the chaotic series, f_s is the central switching frequency, and Δf is the changing range of switching frequencies. Since the chaotic series $\{x_i\}$ are distributed evenly within (0, 1), there are infinite values within the pool of $(f_s - \Delta f/2, f_s + \Delta f/2)$ for switching frequencies.

Figure 10 shows the principle of the discretely chaotic modulation strategy. Also, the switching pulses are generated by comparing the chaotic-frequency sawtooth carrier wave with a constant value of 0.5. Different from the continuously chaotic modulation, there are finite candidates for the switching frequencies. As shown in Figure 10, there are four switching frequency values f_{s1}, f_{s2}, f_{s3} and f_{s4} , and they are adopted when chaotic series $\{x_i\}$ is located within the domains of $[0, 0.25)$, $[0.25, 0.5)$, $[0.5, 0.75)$ and $[0.75, 1)$, respectively.

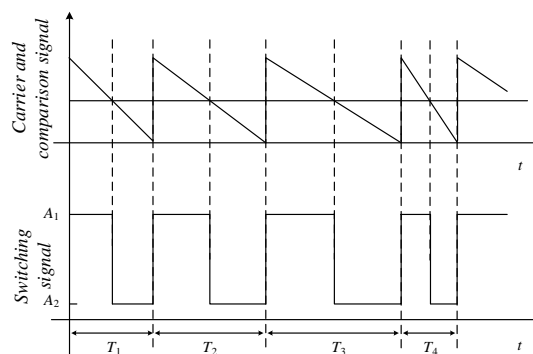


Figure 9. Principle of continuously chaotic modulation.

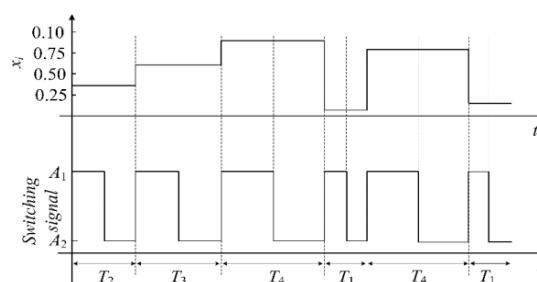


Figure 10. Principle of discretely chaotic modulation.

3.3. Chaotic Modulation for TPI Bidirectional DC/DC Converter

Since there are three full-bridge converters in the TPI bidirectional DC/DC converter, the chaotic switching modulation should be applied for the three ports collaboratively. As shown in Figure 11, if the chaotic modulation is applied for the three ports independently, the desired shifted-phase angles cannot be achieved due to the irregular changes of the switching frequencies. On the other hand, the

shifted-phase angles can be maintained when the synchronously chaotic switching frequencies are used, as shown in Figure 12. Thus, not only the feature of continuous spectrum is provided with chaotic switching frequencies, but also the shifted-phase angle control can be implemented.

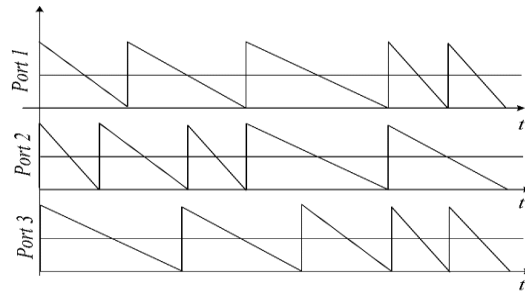


Figure 11. Independently chaotic modulation.

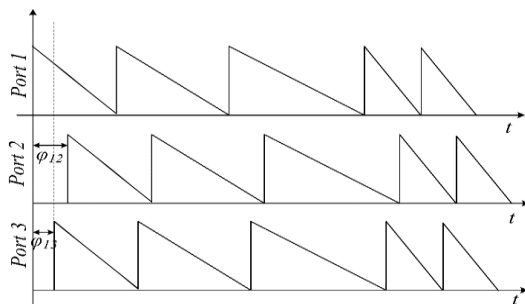


Figure 12. Synchronously chaotic modulation.

4. Control Scheme Based on Chaotic Modulation

Figure 13 shows the chaotic modulation based control of TPI bidirectional DC-DC converter. The closed-loop control of DC link voltage U_o in port 2 generates the shifted-phase angle between port 1 and port 2, namely ϕ_{12} . On the other hand, the closed-loop control of the active power in port 1 produces the shifted-phase angle between port 1 and port 3, namely ϕ_{13} . The active power P_i of port 1 could be calculated by multiplying the converter output voltage u_1 and the input current i_1 on port 1. Then, the switching pulses are generated for three ports with the shifted-phase angles ϕ_{12} and ϕ_{13} , and the synchronously chaotic modulation is applied for the three ports. As mentioned above, the phase-shifted PWM could be applied for the isolated DC/DC converter to extend the soft-switching operation region and increase the converter efficiency [25,26]. For the phase-shifted PWM control, the duty ratio D is added to the switching pulse of port 1.

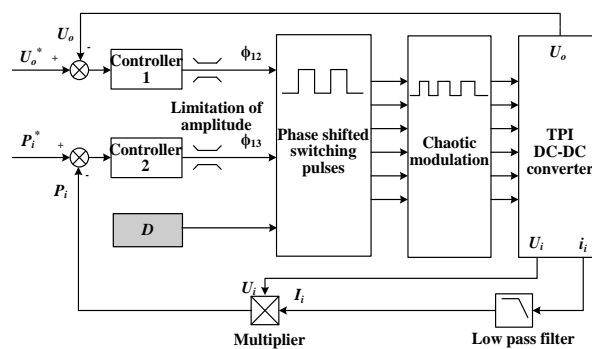


Figure 13. Block diagram of chaotic modulation based control for TPI bidirectional DC/DC converter.

Figure 14 plots the flow chart of digital implementation for the chaotic modulation based control scheme. The switching periods and control parameters are updated in the PWM interrupt program, which is started by the PWM module on port 1. In the PWM interrupt program, the chaotic switching periods ΔT are generated, and they are initially loaded to the period registers for the three ports. After starting AD conversion, the output voltage on port 2 and the input power on port 1 are sensed, which are input to closed-loop controllers to produce the shifted-phase angles ϕ_{12} and ϕ_{13} , respectively. Together with the duty ratio D , the values of ϕ_{12} and ϕ_{13} are loaded to the phase registers of PWM module 2 and PWM module 3, in such a way that the corresponding switching pulses are generated.

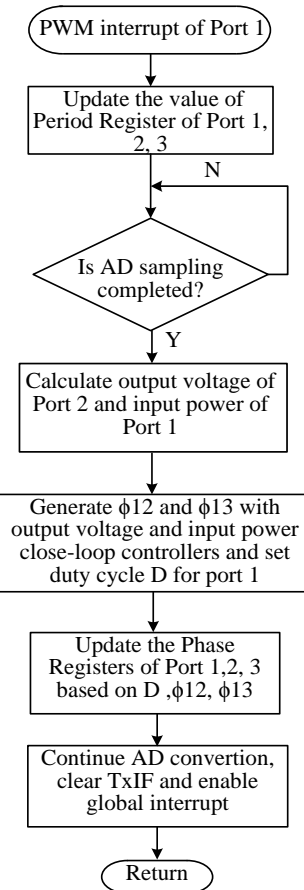


Figure 14. Flow chart of digital implementation for chaotic modulation based control for TPI bidirectional DC/DC converter.

The proportional-integral (PI) controllers are used for the closed-loop control to generate the shifted phase angles among three ports. Their digital expressions are given as:

$$\varphi_{12} = k_{p1}(U_o^* - U_o) + k_{i1} \sum (U_o^* - U_o)\Delta T \quad (6)$$

$$\varphi_{13} = k_{p2}(P_i^* - P_i) + k_{i2} \sum (P_i^* - P_i)\Delta T \quad (7)$$

where k_{p1} and k_{i1} are the proportional and integral coefficients of controller for port 2, and k_{p2} and k_{i2} are the proportional and integral coefficients of controller for port 3. ΔT is the switching period, which varies chaotically. To guarantee good DC output performance of the TPI bidirectional DC/DC converter, the integral coefficients should be updated according to the changing switching periods.

5. Simulation and Experimental Verification

Both simulation and experiments are given to verify the performance of the proposed modulation strategies and control scheme. Firstly, the simulation on a 10-kW TPI bidirectional DC/DC converter is given. The simulation parameters are listed in Table 1. Figure 15 shows the simulated waveforms of TPI bidirectional DC/DC converter using shifted-angle based control with fixed switching frequency. Figure 15a shows the waveforms of converter voltage u_1 and current i_1 of port 1, and the output voltage U_o of port 2. Figure 15b shows the waveforms of converter voltages u_1 , u_2 and u_3 in three ports. The switching period is kept constant at a value T , which is equal to 50 μ s.

Table 1. Simulation parameters.

Quantity	Value
Switching frequency f	20 kHz
Input voltage U_i	288 V
Battery voltage U_b	48 V
Output voltage U_o	288 V
Inductor L_1	32.4 μ H
Inductor L_2	32.4 μ H
Inductor L_3	0.9 μ H
Ratio of transformer $N_1:N_2:N_3$	6:6:1
Resistor load R	8.3 Ω
DC link capacitor C	1000 μ F

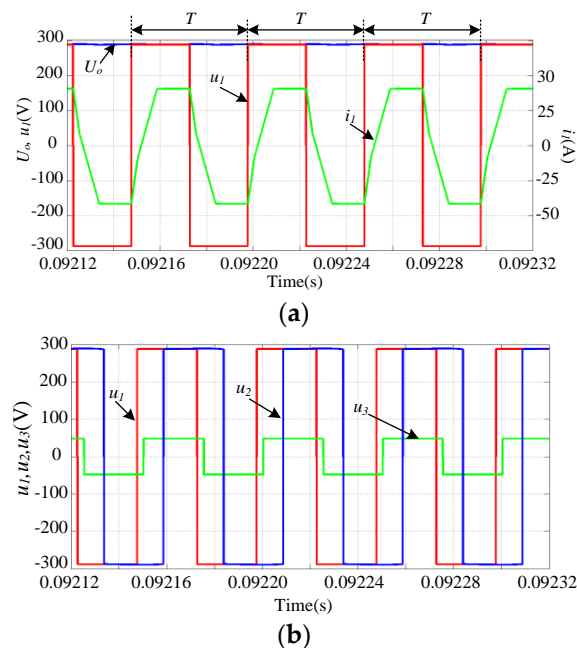


Figure 15. Simulated waveforms of shifted-phase angle control with fixed switching-frequency: (a) converter voltage, current of port 1 and output voltage of port 2; (b) converter voltages of port 1, 2 and 3.

Figure 16 plots the simulated waveforms with shifted-angle based control using continuously chaotic modulation. The expected central switching frequency f_s is set as 20 kHz and the chaotic bandwidth Δf is 2 kHz. There are infinite values for switching frequencies between 18 kHz and 20 kHz. Figure 17 shows the simulated waveforms using discretely chaotic modulation, where four different switching frequencies (18 kHz, 19.3 kHz, 20.6 kHz and 22 kHz) are used alternatively. It is observed that the switching periods are changed irregularly in Figures 16 and 17. Although the

switching periods vary chaotically, the output DC link voltage U_o of port 2 is kept stable with the shifted-phase angle control and chaotic modulation. Actually, no distinct difference can be observed in the output DC link voltage U_o between the fixed frequency modulation and the chaotic modulation strategies. It verifies that chaotic modulation only affects the high-frequency characteristics and does not deteriorate the low-frequency operating performance of the TPI bidirectional DC/DC converter.

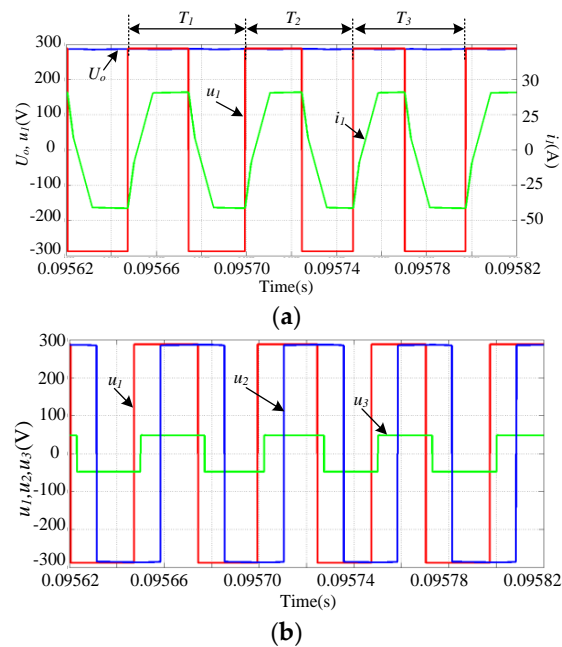


Figure 16. Simulated waveforms of shifted-phase angle control with continuously chaotic modulation: (a) converter voltage, current of port 1 and output voltage of port 2; (b) converter voltages of port 1, 2 and 3.

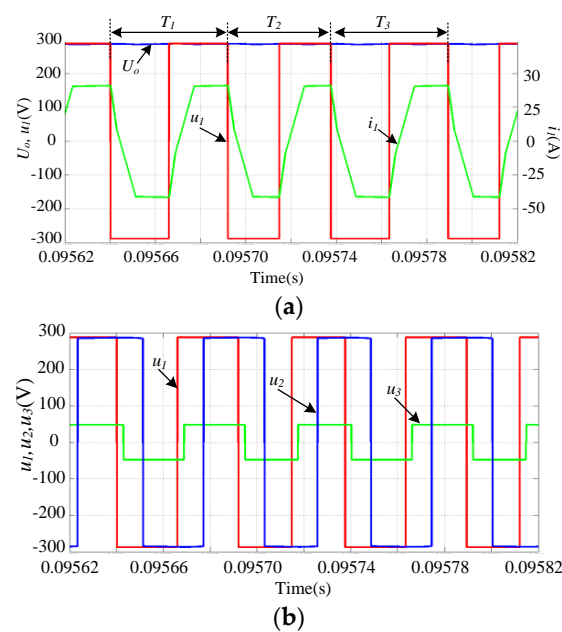


Figure 17. Simulated waveforms of shifted-phase angle control with discretely chaotic modulation: (a) converter voltage, current of port 1 and output voltage of port 2; (b) converter voltages of port 1, 2 and 3.

Figures 18–20 show the simulated waveforms of the phase-shifted PWM controlled TPI bidirectional DC/DC converter using fixed switching frequency, continuously chaotic modulation and discretely chaotic modulation, respectively. The value of duty ratio for converter in port 1 is 0.75. It is observed that both the continuously chaotic modulation and the discretely chaotic modulation produce chaotic waveforms while keeping U_o stable.

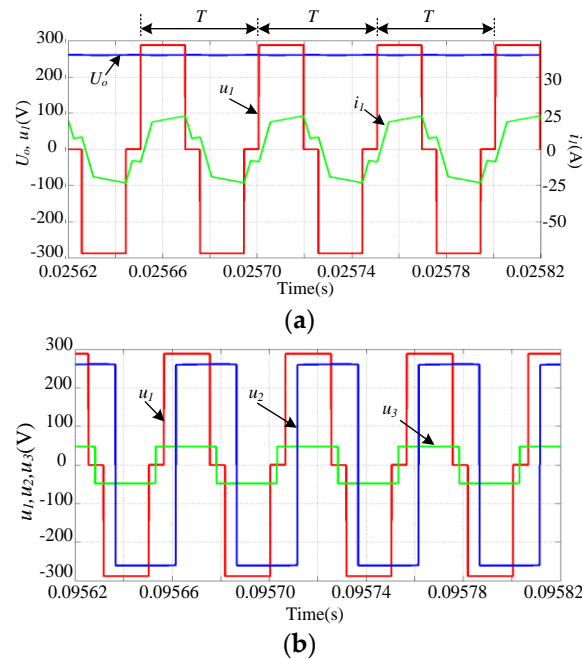


Figure 18. Simulated waveforms of phase-shifted PWM control with fixed switching-frequency: (a) converter voltage, current of port 1 and output voltage of port 2; (b) converter voltages of port 1, 2 and 3.

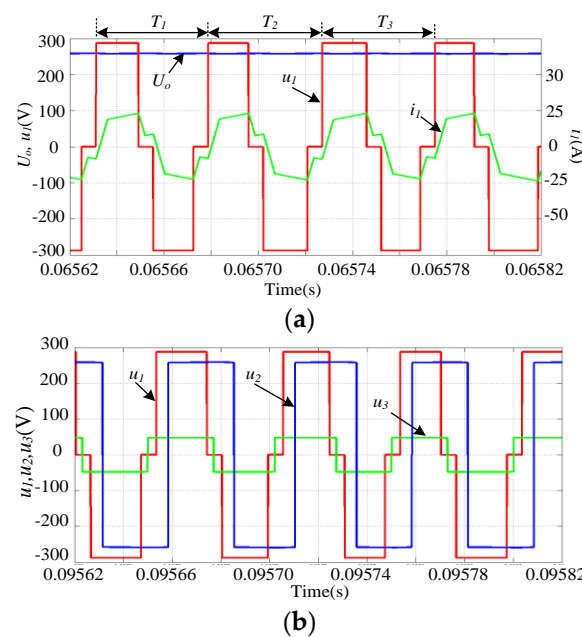


Figure 19. Simulated waveforms of phase-shifted PWM control with continuously chaotic modulation: (a) converter voltage, current of port 1 and output voltage of port 2; (b) converter voltages of port 1, 2 and 3.

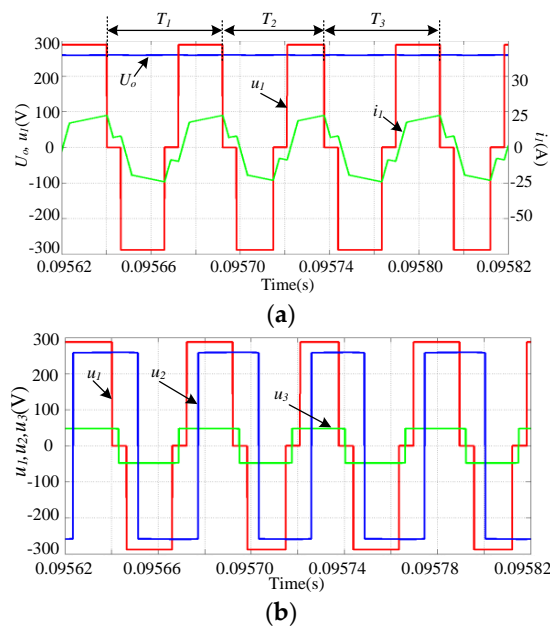


Figure 20. Simulated waveforms of phase-shifted PWM control with discretely chaotic modulation: (a) converter voltage, current of port 1 and output voltage of port 2; (b) converter voltages of port 1, 2 and 3.

Then, the experiments are carried out on a small-power laboratory prototype to verify the performance of the proposed modulation strategies and control scheme for TPI bidirectional DC/DC converter. The experimental parameters are listed in Table 2. It should be noted that the rated voltage and power of the prototype are lower compared to those in practical energy conversion systems of EVs and HEVs, but the purpose of the experiments is to verify the validity of the proposed modulation and control for TPI bidirectional DC/DC converter. Therefore, the low-power prototype could still be used. Power MOSFETs (IPW65R019C7) and the driver chip HCPL3120 are adopted for the power switches in the experiments. The DSP TI-TMS320F28335 is used as the digital controller to implement the control algorithm and generate the switching pulses. The voltage sensors (LEM LV25-P, LEM, Beijing, China) and the current sensors (LEM LA25-NP, LEM, Beijing, China) are used to measure the voltages and currents. The three-port high-frequency transformer is made by choosing proper magnetic cores and copper wires.

Table 2. Experimental parameters.

Quantity	Value
Switching frequency f	20 kHz
Input voltage U_i	50 V
Battery voltage U_b	12 V
Output voltage U_o	65 V
Inductor L_1	101 μ H
Inductor L_2	206 μ H
Inductor L_3	29 μ H
Ratio of transformer $N_1:N_2:N_3$	5:7:1
Resistor load R	60 Ω
DC link capacitor C	1000 μ F

Figures 21–23 show the measured waveforms of TPI bidirectional DC/DC converter with shifted-phase angle control in experiments. The switching period is kept constant as T with fixed switching-frequency in Figure 21. Different from that, the switching periods change chaotically using

continuously chaotic modulation in Figure 22 and using discretely chaotic modulation in Figure 23, respectively. Although the high-frequency behaviors are irregular using chaotic modulation, the output voltage of U_o in port 2 is kept stable in Figures 22 and 23. To show the improved spectrum performance, Figure 24 plots the power spectrum of the DC link current of port 1 using different modulation strategies. It is observed clearly that distinct peaky harmonics exist around 4 kHz and its multiple frequencies using fixed switching-frequency in Figure 24a. Differently, the peaky switching harmonics are reduced for around 10 dB in spectrum by using continuously chaotic modulation in Figure 24b and using discretely chaotic modulation in Figure 24c. The reason lies in that the power of switching harmonics is spread out within the nearby frequency domain in spectrum.

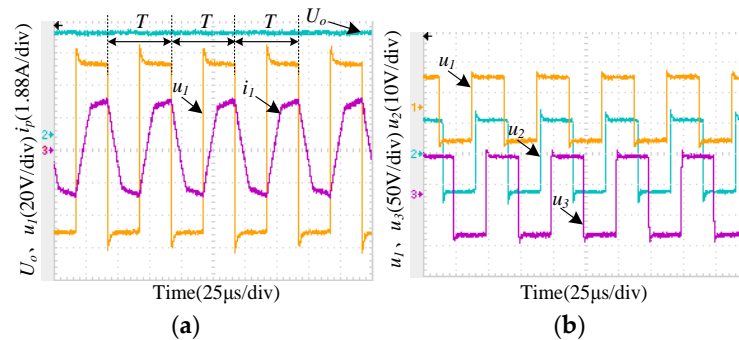


Figure 21. Measured waveforms of shifted-phase angle control using fixed switching-frequency: (a) converter voltage, current of port 1 and output voltage of port 2; (b) converter voltages of port 1, 2 and 3.

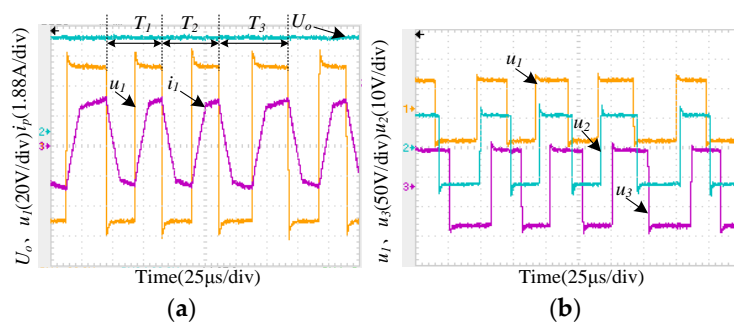


Figure 22. Measured waveforms of shifted-phase angle control using continuously chaotic modulation: (a) converter voltage, current of port 1 and output voltage of port 2; (b) converter voltages of port 1, 2 and 3.

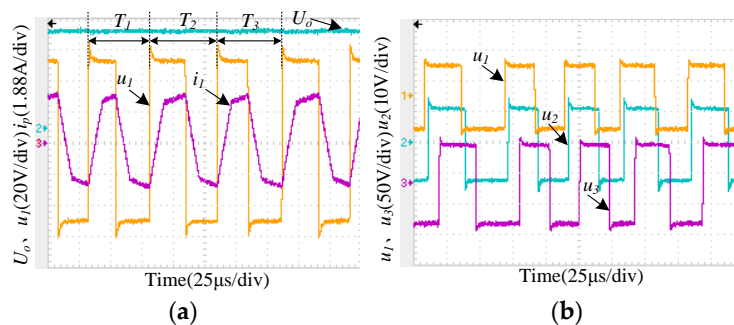


Figure 23. Measured waveforms of shifted-phase angle control using discretely chaotic modulation: (a) converter voltage, current of port 1 and output voltage of port 2; (b) converter voltages of port 1, 2 and 3.

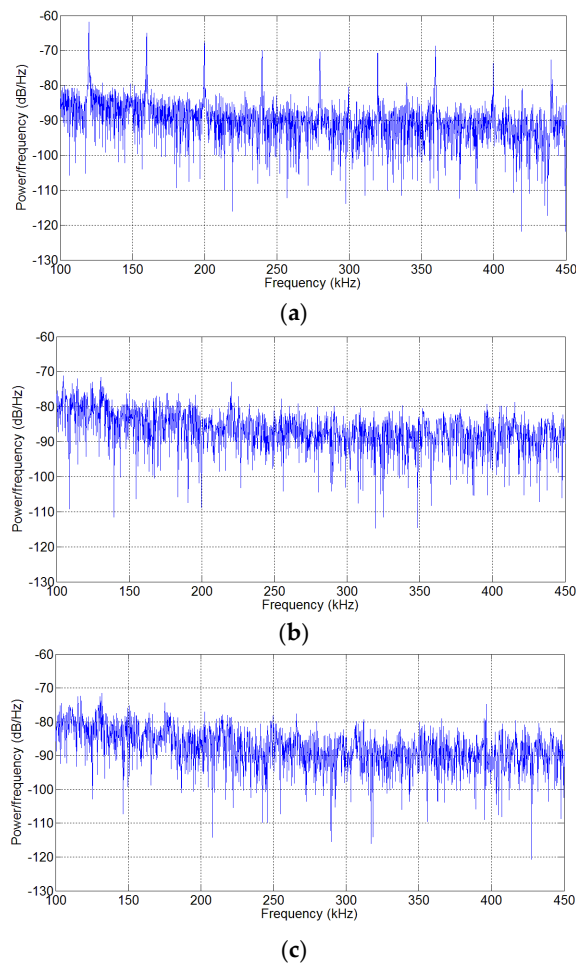


Figure 24. Measured power spectrum density of shifted-phase angle control: (a) fixed switching-frequency; (b) continuously chaotic modulation; (c) discretely chaotic modulation.

The experimental verification is also given for the TPI bidirectional DC/DC converter with phase-shifted PWM control. The measured waveforms using fixed switching-frequency, continuously chaotic modulation and discretely chaotic modulation are shown in Figures 25–27 respectively. The chaotic modulation schemes can keep the output voltage U_o stable in port 2 although they exhibit chaotic behaviors in high-frequency domain.

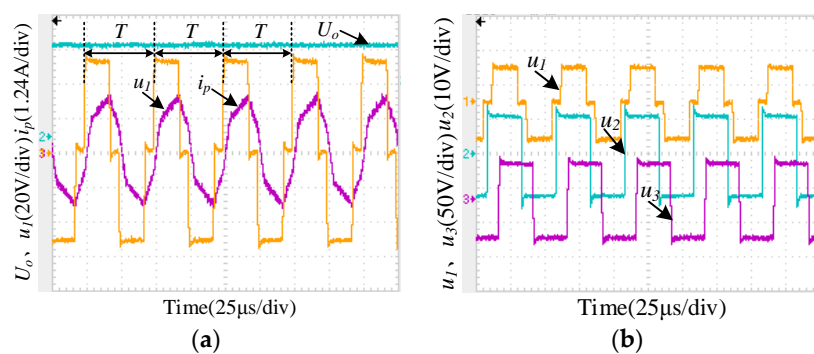


Figure 25. Measured waveforms of phase-shifted PWM control using fixed switching frequency: (a) converter voltage, current of port 1 and output voltage of port 2; (b) converter voltages of port 1, 2 and 3.

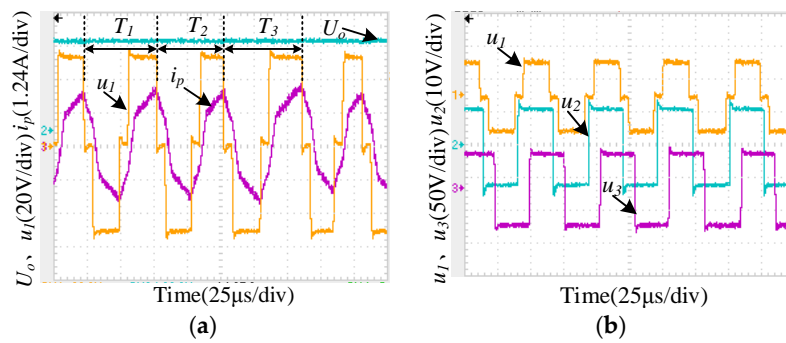


Figure 26. Measured waveforms of phase-shifted PWM control using continuously chaotic modulation: (a) converter voltage, current of port 1 and output voltage of port 2; (b) converter voltages of port 1, 2 and 3.

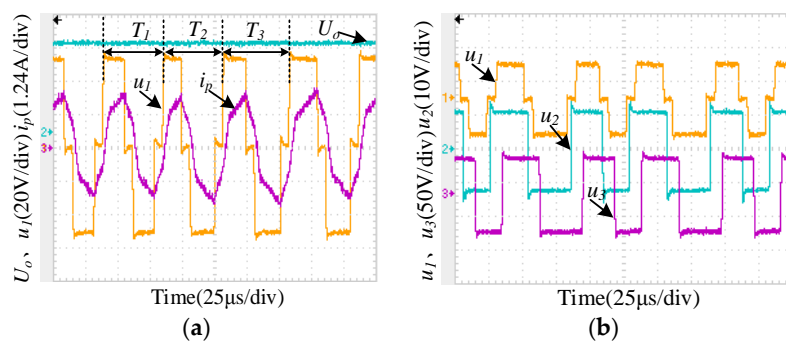


Figure 27. Measured waveforms of phase-shifted PWM control using discretely chaotic modulation: (a) converter voltage, current of port 1 and output voltage of port 2; (b) converter voltages of port 1, 2 and 3.

The spectrum comparison of DC link current in port 1 is presented among different switching strategies for the phase-shifted PWM control in Figure 28. In Figure 28a, the distinct switching harmonics are observed in the spectrum using fixed switching-frequency. Those harmonic peaks may introduce the conducted EMI in EVs and HEVs. By using chaotic modulation, the switching harmonics are reduced for around 10 dB in Figure 28b,c. It verifies that the conducted EMI issue can be mitigated effectively by using chaotic modulation strategies. As mentioned in Section 3, the simple Logistic map is used to generate the iterative series for chaoticizing the switching frequency. Therefore, no additional hardware is needed for the proposed chaotic modulation, and the system cost is the same as that with fixed switching-frequency.

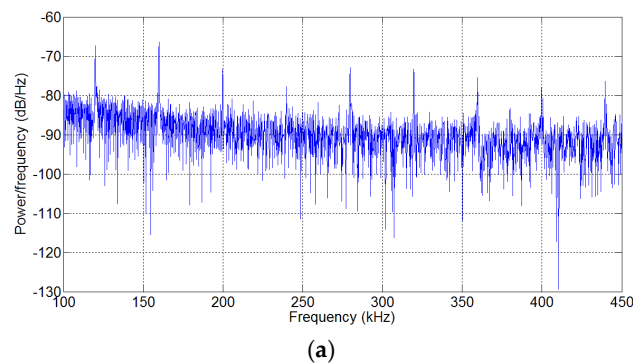


Figure 28. Cont.

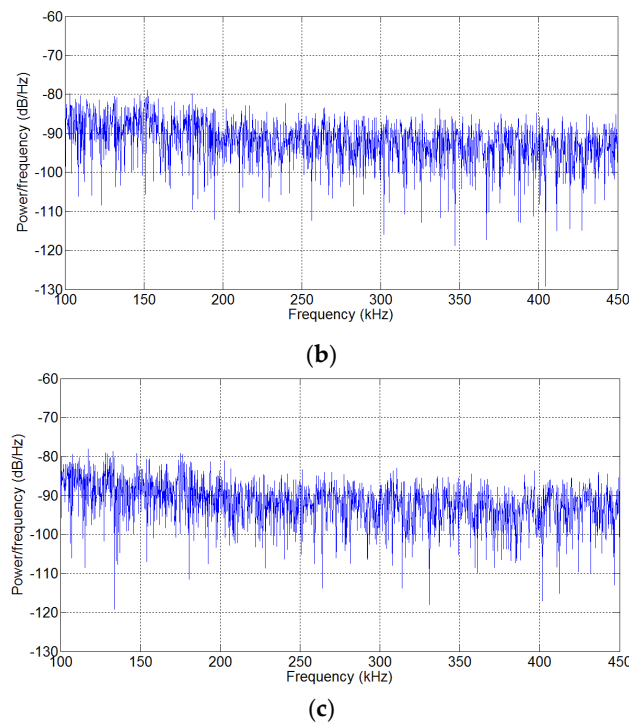


Figure 28. Measured power spectrum density of phase-shifted PWM control: (a) fixed switching-frequency; (b) continuously chaotic modulation; (c) discretely chaotic modulation.

6. Conclusions

In this paper, the chaotic modulation strategies and the related control schemes are presented for TPI bidirectional DC/DC converters, which could be used in electric and hybrid vehicles. Two chaotic modulation strategies, namely the continuously chaotic modulation and the discretely chaotic modulation are proposed. With conventional fixed-frequency modulation, distinct harmonic peaks exist around the switching frequency and its multiple values in the spectrum, which may induce conducted EMI in electric and hybrid vehicles. Different from that, the switching frequencies of the proposed chaotic modulation strategies are changed irregularly for TPI bidirectional DC/DC converters. The power clustered around the switching frequency and its multiple values are thus spread out within the nearby frequency domain, and the switching harmonic peaks are suppressed. Our experiments on a small-power laboratory prototype verify that the proposed chaotic modulation strategies can reduce the switching harmonic peaks for around 10 dB in spectrum. Therefore, the conducted EMI induced by the high-frequency switching harmonics is mitigated effectively. The average switching frequency is as high as 20 kHz, and the chaotic change of switching frequency will not deteriorate the DC output performance of TPI bidirectional DC/DC converter.

On the other hand, the proposed chaotic modulation strategies for TPI bidirectional DC/DC converters have the same hardware compared to the conventional fixed-frequency modulation. The chaotic modulation algorithms can be implemented easily with the digital controller. The one-dimensional logistic map is used to generate the chaotic series, which in turn generates the irregular switching frequencies for TPI bidirectional DC/DC converters. Therefore, the proposed strategies can provide better spectrum performance for TPI bidirectional DC/DC converters without increasing the system cost.

Acknowledgments: This work was supported in part by the National Key Basic Research Program of China (973 program) under Grant 2013CB035603, in part by the National Natural Science Foundation of China under Grant 51577027, in part by the Aeronautical Science Foundation of China under Grant 20142869014, and in part by Jiangsu Province Qin Lan Project (1116000195).

Author Contributions: Zheng Wang proposed the idea, designed the method and wrote the paper; Bochen Liu designed and did the experiments; Yue Zhang and Kai Chu participated in building the experimental setup and analyzing the data; Ming Cheng contributed verifying validity of the method.

Conflict of Interest: The authors declare no conflicts of interests.

References

1. Woo, D.G.; Joo, D.M.; Lee, B.K. On the feasibility of integrated battery charger utilizing traction motor and inverter in plug-in hybrid electric vehicles. *IEEE Trans. Power Electron.* **2015**, *30*, 7270–7281. [[CrossRef](#)]
2. Xue, L.X.; Shen, Z.Y.; Boroyevich, D.; Mattavelli, P.; Diaz, D. Dual active bridge-based battery charger for plug-in hybrid electric vehicle with charging current containing low frequency ripple. *IEEE Trans. Power Electron.* **2015**, *30*, 7299–7307. [[CrossRef](#)]
3. Chau, K.T.; Chan, C.C. Emerging energy-efficient technologies for hybrid electric vehicles. *Proc. IEEE* **2007**, *75*, 821–835. [[CrossRef](#)]
4. Van Roy, J.; Leemput, N.; Geth, F.; Buscher, J.; Salenbien, R.; Driesen, J. Electric vehicle charging in an office building microgrid with distributed energy resources. *IEEE Trans. Sustain. Energy* **2014**, *5*, 1389–1396. [[CrossRef](#)]
5. Lai, J.S.; Nelson, D.J. Energy management power converters in hybrid electric and fuel cell vehicles. *Proc. IEEE* **2007**, *95*, 766–777. [[CrossRef](#)]
6. Ehsani, M.; Gao, Y.; Miller, J.M. Hybrid electric vehicles: Architecture and motor drives. *Proc. IEEE* **2007**, *95*, 719–728. [[CrossRef](#)]
7. Veneri, O.; Capasso, C.; Iannuzzi, D. Experimental evaluation of DC charging architecture for fully-electrified low-power two-wheeler. *Appl. Energy* **2016**, *162*, 1428–1438. [[CrossRef](#)]
8. Capasso, C.; Veneri, O. Experimental study of a DC charging station for full electric and plug in hybrid vehicles. *Appl. Energy* **2015**, *152*, 131–142. [[CrossRef](#)]
9. Xu, D.; Zhao, C.; Fan, H. A PWM plus phase-shift control bidirectional DC-DC converter. *IEEE Trans. Power Electron.* **2004**, *19*, 666–675. [[CrossRef](#)]
10. Tan, N.M.L.; Abe, T.; Akagi, H. Design and performance of a bidirectional isolated DC-DC converter for a battery energy storage system. *IEEE Trans. Power Electron.* **2012**, *27*, 1237–1248. [[CrossRef](#)]
11. Chen, G.; Lee, Y.S.; Hui, S.Y.R.; Xu, D.; Wang, Y. Actively clamped bidirectional flyback converter. *IEEE Trans. Ind. Electron.* **2000**, *47*, 770–779. [[CrossRef](#)]
12. Swingler, A.D.; Dunford, W.G. Development of a bi-directional DC/DC converter for inverter/charger applications with consideration paid to large signal operation and quasi-linear digital control. In Proceedings of the IEEE Power Electronics Specialists Conference, Cairns, Australia, 23–27 June 2002.
13. Li, H.; Peng, F.Z.; Lawler, J.S. A natural ZVS medium-power bidirectional DC-DC converter with minimum number of devices. *IEEE Trans. Ind. Appl.* **2003**, *39*, 525–535. [[CrossRef](#)]
14. Wu, K.Y.; de Silva, C.W.; Dunford, W.G. Stability analysis of isolated bidirectional dual active full-bridge DC-DC converter with triple phase-shift control. *IEEE Trans. Power Electron.* **2012**, *27*, 2007–2017. [[CrossRef](#)]
15. Di Napoli, A.; Crescimbeni, F.; Rodo, S.; Solero, L. Multiple input DC-DC power converter for fuel-cell powered hybrid vehicles. In Proceedings of the 33rd Annual IEEE Power Electronics Specialists Conference, Cairns, Australia, 23–27 June 2002.
16. Su, G.J.; Peng, F.Z. A low cost, Triple-voltage bus DC/DC converter for automotive application. In Proceedings of the IEEE Applied Power Electronics Conference and Exposition (APEC), Austin, TX, USA, 6–10 March 2005.
17. Tao, H.; Kotsopoulos, A.; Duarte, J.L.; Hendrix, M.A.M. Multi-input bidirectional DC-DC converter combining DC-link and magnetic-coupling for fuel cell systems. In Proceedings of the IEEE Industry Applications Society Conference (IAS), Hong Kong, China, 2–6 October 2005.
18. Michon, M.; Duarte, J.L.; Hendrix, M.; Simoes, M.G. A three-port bi-directional converter for hybrid fuel cell systems. In Proceedings of the IEEE Power Electronics Specialists Conference, Aachen, Germany, 20–25 June 2004.
19. Tao, H.; Duarte, J.L.; Hendrix, M.A.M. Three-port triple-half-bridge bidirectional converter with zero-voltage switching. *IEEE Trans. Power Electron.* **2008**, *23*, 782–792.

20. Zhao, C.H.; Round, S.D.; Kolar, J.W. An isolated three-port bidirectional DC-DC converter with decoupled power flow management. *IEEE Trans. Power Electron.* **2008**, *23*, 2443–2453. [[CrossRef](#)]
21. Kim, S.Y.; Song, H.S.; Nam, K. Idling port isolation control of three-port bidirectional converter for EVs. *IEEE Trans. Power Electron.* **2012**, *27*, 2495–2506. [[CrossRef](#)]
22. Lai, Y.S.; Chen, B.Y. New random PWM technique for a full-bridge DC/DC converter with harmonic intensity reduction and considering efficiency. *IEEE Trans. Power Electron.* **2013**, *28*, 5013–5023. [[CrossRef](#)]
23. Ho, E.N.Y.; Mok, P.K.T. Design of PWM ramp signal in voltage-mode CCM random switching frequency buck converter for conductive EMI reduction. *IEEE Trans. Circuits Syst. I Regul. Papers* **2013**, *60*, 505–515. [[CrossRef](#)]
24. Liaw, C.M.; Lin, Y.M.; Wu, C.H.; Hwu, K.I. Analysis, design, and implementation of a random frequency PWM inverter. *IEEE Trans. Power Electron.* **2000**, *15*, 843–854. [[CrossRef](#)]
25. Oggier, G.G.; Ledhold, R.; Garcia, G.O.; Oliva, A.R.; Balda, J.C.; Barlow, F. Extending the ZVS operating range of dual active bridge high-power DC-DC Converters. In Proceedings of the Power Electronics Specialists Conference, Jeju, Korea, 18–22 June 2006.
26. Zhao, B.; Song, Q.; Liu, W.; Liu, G.; Zhao, Y. Universal high-frequency-link characterization and practical fundamental-optimal strategy for dual-active-bridge DC-DC converter under PWM plus phase-shift control. *IEEE Trans. Power Electron.* **2015**, *30*, 6488–6494. [[CrossRef](#)]



© 2016 by the authors; licensee MDPI, Basel, Switzerland. This article is an open access article distributed under the terms and conditions of the Creative Commons by Attribution (CC-BY) license (<http://creativecommons.org/licenses/by/4.0/>).